Microstructure and magnetism of Co_2FeAl Heusler alloy prepared by arc and induction melting compared with planar flow casting

A. Titov, Y. Jiraskova, O. Zivotsky, J. Bursik, and D. Janickovic

Citation: AIP Advances **8**, 047206 (2018); doi: 10.1063/1.4993698
View online: https://doi.org/10.1063/1.4993698
View Table of Contents: http://aip.scitation.org/toc/adv/8/4
Published by the American Institute of Physics

AIP ADVANCES **8**, 047206 (2018)

Microstructure and magnetism of Co_2FeAl Heusler alloy prepared by arc and induction melting compared with planar flow casting

A. Titov,[1,2,a] Y. Jiraskova,[2,3] O. Zivotsky,[1] J. Bursik,[3] and D. Janickovic[4]
[1]*Department of Physics, VSB-Technical University of Ostrava, Ostrava-Poruba 708 33, Czech Republic*
[2]*CEITEC IPM, Institute of Physics of Materials, AS CR, Brno 616 62, Czech Republic*
[3]*Institute of Physics of Materials, AS CR, Brno 616 62, Czech Republic*
[4]*Institute of Physics, Slovak Academy of Sciences, Bratislava 845 11, Slovakia*

(Received 30 June 2017; accepted 2 October 2017; published online 19 October 2017)

This paper is devoted to investigations of the structural and magnetic properties of the Co_2FeAl Heusler alloy produced by three technologies. The alloys prepared by arc and induction melting have resulted in coarse-grained samples in contrast to the fine-grained ribbon-type sample prepared by planar flow casting. Scanning electron microscopy completed by energy dispersive X-ray spectroscopy, X-ray diffraction, Mössbauer spectroscopy, and magnetic methods sensitive to both bulk and surface were applied. The chemical composition was slightly different from the nominal only for the ribbon sample. From the viewpoint of magnetic properties, the bulk coercivity and remnant magnetization have followed the structure influenced by the technology used. Saturation magnetization was practically the same for samples prepared by arc and induction melting, whereas the magnetization of ribbon is slightly lower due to a higher Al content at the expense of iron and cobalt. The surface magnetic properties were markedly influenced by anisotropy, grain size, and surface roughness of the samples. The surface roughness and brittleness of the ribbon-type sample did not make domain structure observation possible. The other two samples could be well polished and their highly smooth surface has enabled domain structure visualization by both magneto-optical Kerr microscopy and magnetic force microscopy.
https://doi.org/10.1063/1.4993698

I. INTRODUCTION

The Heusler alloys still attract remarkable attention regarding various compositions, physical properties, and subsequent applications.[1] This is documented by an increasing number of scientific papers in recent years, about 500 in total. The Heusler alloys are characterized by the formula X_2YZ, where X and Y are transition metals (e.g. Fe, Co, Mn) and Z is an element from a group III, IV, or V. Basically, this formula consists of two binary B2 compounds XY and XZ both of CsCl type crystal structure. This means that an ability of a compound to form the B2 structure can also indicate the possibility to form a Heusler alloy. Among a huge number of various compositions, the Co-based Heusler compounds are of particular interest because they are good ferromagnetic materials, show comparatively high Curie temperatures, up to 1000 K, and have relatively low degrees of atomic disordering.[2] Moreover, it was reported that their tunnelling magnetoresistance can exceed up to 1000%.[3,4] This makes Heusler-based devices attractive for magnetic data storage applications.

At present, Co_2FeAl belongs to one of the most studied Heusler alloys. It provides huge tunnelling magnetoresistance ratio in magnetic tunnel junctions[5,6] but also a low Gilbert damping[7] essential for

[a]Corresponding author. Email: andrii.titov@vsb.cz

spin switching with low currents and spin torque oscillators. The use of Co_2FeAl as a ferromagnetic material in spintronic devices requires deep knowledge and control of its magnetic properties. One of the key parameters is magnetic anisotropy, which is directly related to the spin-orbit-coupling relativistic effect. Magnetic anisotropy and its changes can be effectively modified by microstructure and thereby also by a modification of the electronic structure in bulk, surface and/or interfaces.

There are several ways to synthesize Heusler alloys. Beside conventional techniques (e.g., arc melting, commercial induction furnace melting of stoichiometric amounts of the constituents in a protective noble gas atmosphere into a form of bulk compounds,[8] mechanical alloying method,[9,10] molecular beam epitaxy,[11] chemical route,[12] electrospinning method,[13] co-precipitation route,[14] etc.), there is ongoing effort to search for non-traditional preparation technologies which could produce Heusler alloys with improved properties. This is also the case of the present study. The conventional arc and induction melting technologies were completed by the planar flow casting technology known from the preparation of amorphous and/or nanocrystalline materials into a ribbon form.

II. EXPERIMENTAL

A. Sample preparation

Co_2FeAl Heusler alloys were prepared from high-purity elements: Fe – 99.95%, Co – 99.8%, and Al – 99.95%. Arc melting (AM) using a MAM-1 furnace (Buehler GmbH) and induction melting (IM) were used for the production of button- and cylindrical-type ingots. Each arc-melted ingot was melted four times to guarantee a good homogeneity; the weight loss was close to 1%. The ingots were cut using spark erosion in deionized water into discs about 500 μm thick. The surface of the disc-sample was first grinded and polished to remove oxides. Subsequently, the samples, denoted DAM and DIM, respectively, were polished using Vibromet for 24 h to guarantee the best possible surface smoothness. One cylindrical type ingot was used for the preparation of 2 mm wide and 20 μm thick ribbons using planar flow casting procedure. This sample is denoted by R. The high surface roughness of the ribbon and impossibility of polishing owing to high brittleness were the limitations for the surface sensitive magneto-optical and atomic force microscope observation.

B. Experimental methods

1. Scanning electron microscopy (SEM)

A TESCAN LYRA 3XMU FEG/SEM scanning electron microscope working at accelerating voltage of 20 kV equipped with an XMax80 Oxford Instruments detector for energy dispersive X-ray analysis (EDX) was used to follow the morphology and microstructure.

2. X-ray diffraction (XRD)

An X'PERT PRO diffractometer with Co Kα radiation (λ = 0.17902 nm) was used to study the structural and compositional properties. The X-ray diffractograms were measured at room temperature (RT) from $2\theta = 35°$ to 135° in steps of 0.008° and 500 s per deg. The analysis of powder patterns was realized by HighScore Plus program using the Rietveld structure refinement method[15] and the ICSD database of inorganic and related structures.[16] Besides the lattice parameters of the analyzed phases, the size of coherently diffracting domains and microstrains were obtained from the pattern analysis.

3. Mössbauer spectrometry (MS)

^{57}Fe Mössbauer spectrometry was used to gain insight into the structural evolution of the local environment of the iron atoms. The measurements were carried out at RT using a ^{57}Co(Rh) source. Standard transmission geometry was applied for the ribbon-type R sample; backscattering geometry using γ-rays for the disc-type, DAM and DIM, samples. The calibration of velocity scales in both measuring geometries was performed with α-Fe and the isomer shifts are given with respect to the RT Mössbauer spectrum of α-Fe. All spectra were measured with nearly the same quality and evaluated within the transmission integral approach using the CONFIT program.[17] In the measured Mössbauer spectrum, the crystalline components are represented by discrete single-, double-, and/or six-line

Lorentzian sub-spectra determined by discrete values of hyperfine parameters: δ - isomer shift(s), Δ - quadrupole splitting(s), and B - hyperfine induction(s), corresponding to paramagnetic (δ and Δ) and/or ferromagnetic (δ, Δ, and B) phases, respectively. All components are further described by their intensities, A.

4. Magnetic measurements

a. Bulk magnetic properties. RT hysteresis loops were obtained using a vibrating sample magnetometer (VSM) Microsense EV9 with maximal magnetic field up to 1600 kA/m. The magnetic characteristics, coercivity, remnant and saturation magnetizations were derived from the hysteresis loops with the accuracy of ± 1%. The magnetic measurements were also applied to determine Henkel plots. Typically, they are constructed using isothermal remanence (IRM) and DC demagnetization (DCD) curves.[18] However, some simplifications described in Ref. 19 enable us to obtain the same information using the relation between the initial (virgin) curve, $M_{\mathrm{VIR}}(H)$, and magnetizations at increasing $M_{\mathrm{UP}}(H)$ and decreasing $M_{\mathrm{DOWN}}(H)$ positive magnetic fields:

$$\Delta M(H) = M_{\mathrm{VIR}}(H) - (M_{\mathrm{UP}}(H) + M_{\mathrm{DOWN}}(H))/2. \quad (1)$$

b. Surface magnetic properties. The surface hysteresis loops of all samples (DAM, DIM, and R) were measured using the longitudinal and the polar magneto-optical Kerr effect (MOKE), the red laser diode of 670 nm wavelengths and expressed as the dependence of Kerr rotation on applied magnetic field. The contributions of the in-plane longitudinal magnetization component M_L, parallel to both the applied magnetic field and the plane of incident light, and the out-of-plane polar component M_P, perpendicular to the sample surface, were separated from the loops measured at an oblique incident angle of 50°. These results were confirmed at normal incident geometry, when the polar magnetization component M_P was clearly detected. The surface magnetic domain structure was observed by magneto-optical Kerr microscopy (MOKM) and by magnetic force microscopy (MFM) with NTEGRA Prima platform operated in semi-contact mode.

III. RESULTS AND DISCUSSION

A. Morphology, chemical and phase composition

The morphology of as-prepared samples is shown in Fig. 1. The SEM micrographs of the DAM (a) and DIM (b) samples clearly document their coarse-grained structure. The grain size varies between 300 μm up to 500 μm, whereas the grains in the R sample are substantially smaller, 1-3 μm. The chemical analyses taken from the area of about 1 mm^2 at the DAM and DIM samples and summarized in Table I do not yield any important difference from the nominal composition. A detailed analysis of the individual grains of the DAM sample has pointed at dendrite structure with a slightly higher Al content at the expense of Fe in dendrite cores (48.34 ± 0.23 at.% Co, 22.20 ± 0.46 at.% Fe, 29.46 ± 0.31 at.% Al). Uneven droplet-like and flake-like shapes of R sample pieces did not enable us standard surface polishing; the EDX analyses in this case have larger scatter as it is documented in Table I, last row.

The X-ray diffractograms of DAM and DIM samples show virtually no difference and therefore only the diffraction pattern of the DAM sample is shown in Fig. 2a together with a slightly different

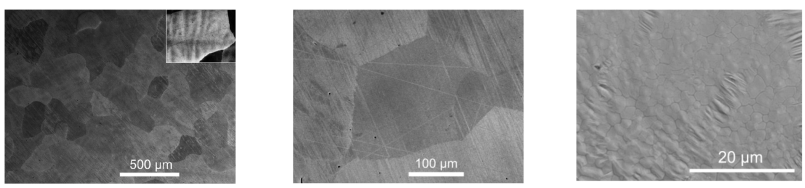

FIG. 1. Surface morphology of the arc melted, DAM, sample and detail (inset) of dendrite structure observed at grains (a); of the induction melted, DIM, sample (b), and of the ribbon, R, sample (c).

TABLE I. Element concentrations obtained by EDX from areas about 1 mm^2.

Sample	Co (at.%)	Fe (at.%)	Al (at.%)
DAM	48.84 ± 0.59	24.06 ± 1.70	27.10 ± 2.11
DIM	49.29 ± 0.21	25.53 ± 0.10	25.18 ± 0.31
R	40.70 ± 2.62	22.21 ± 1.48	37.09 ± 4.02

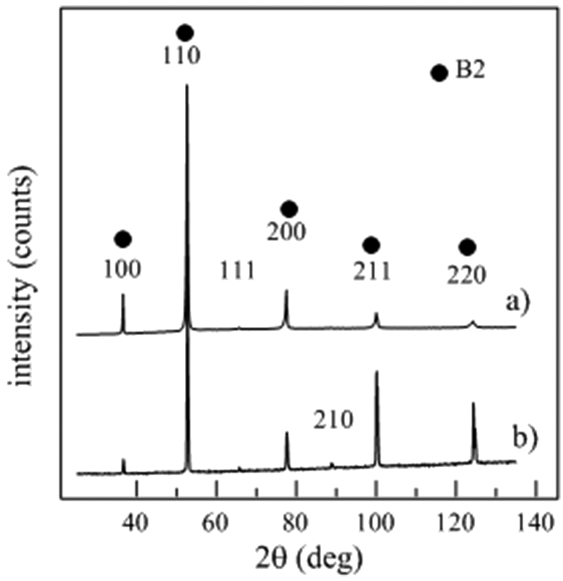

FIG. 2. XRD patterns of arc melted (DAM) sample (a) and ribbon (R) sample (b).

diffraction pattern of the R sample in Fig. 2b. The peaks are labeled by corresponding h, k, l, values. In the full-Heusler alloy of the chemical formula X_2YZ, the ordered $L2_1$ structure (Fig. 3) and two kinds of disordered structures referred to as *B2* (Y-Z disordering) and *A2* (X-YZ disordering) can exist. Based on relations between atomic orderings and superlattice diffraction lines, the patterns can be divided into odd (h, k, l are odd numbers, e.g. (111)), even ((h+k+l)/2 = 2n+1, e.g. (200)),

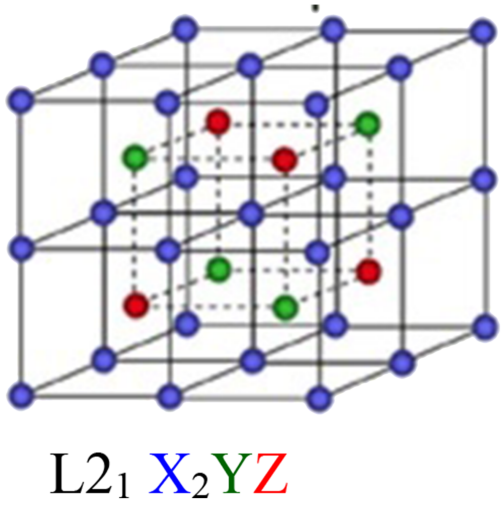

FIG. 3. Schematic representation of the $L2_1$ structure of full-Heusler alloys; the X (Co) atoms are placed on the Wyckoff position 8c, the Y(Fe) and Z(Al) atoms are located on 4a and 4b positions, respectively.

and fundamental (((h+k+l)/2 = 2n, independent of the ordering structures, e.g.(220)) diffraction.[20] The Rietveld analysis of measured data for all samples was done using the ICSD 57 607 database[21] for Co_2FeAl alloy considering the $L2_1$ structure. It has yielded the lattice parameter 0.5733(4) nm for the DAM and DIM samples and 0.5729(3) nm, for the R sample, i.e., virtually identical within an experimental error. A slight difference was obtained only for the coherently diffracting domains size, d (not equivalent to grain size visible in Fig. 1), and lattice microstrain, E. These parameters were determined by comparing the profile width of a standard profile with a sample profile according to the Scherrer formula ($d_{average} = K\lambda/((B_{obs} - B_{std})\cos\theta)$ and according to the tangent formula ($E = \sqrt{(B^2_{obs} - B^2_{std})}/(4\tan\theta)$ using Size/Strain calculator as a part of programs X'Pert Data viewer and HighScorePlus both by Panalytical.[15] The values for DAM and DIM samples were $d = 50 \div 60$ nm and $E = 0.210$ % and for R sample $d = 43$ nm and $E = 0.265$ %. Nevertheless, it turned out that this ICSD 57 607 database is not too satisfactory for analysis of present X-ray patterns. The detected types of superlattice diffraction lines (odd, even, fundamental) have indicated a complex atomic ordering. Its evaluation, i.e., the degree of $B2$-ordering and $L2_1$-ordering has required a more detailed analysis based on traditional analytical approach of Webster,[22] appropriately extended by Takamura.[23] This proceeds at presence and the results, exceeding the scope of this paper, will be published elsewhere.

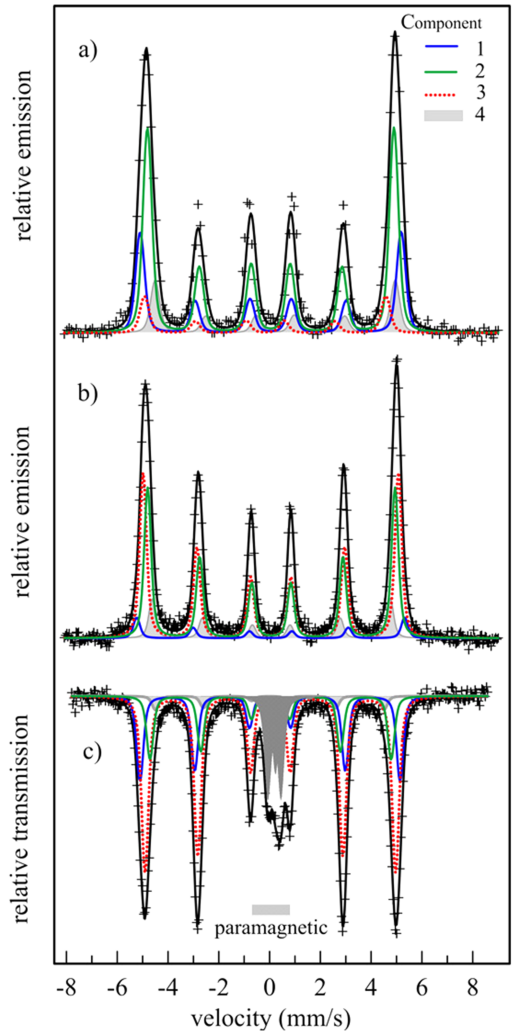

FIG. 4. Mössbauer spectra of the arc melted, DAM, (a), induction melted, DIM, (b), and planar flow casting, R, (c) samples resolved into ferromagnetic (1, 2, 3, 4, see Table II) and paramagnetic (see text) sub-components.

B. Mössbauer spectrometry

Since Mössbauer spectrometry is a highly sensitive method for the study of magnetic properties on an atomic level, it was also applied in the present investigation. The main purpose was to detect atom ordering in the surroundings of resonating Fe atoms and to see fine structural differences between the alloys prepared by various technological conditions. The Co_2FeAl full-Heusler alloy of general formula X_2YZ crystallizes in the $L2_1$ structure consisting of four fcc sublattices shown in Fig. 3.

The resonating Fe atoms have Fe, Co, and Al atoms in their neighborhood; their ordering together with structure defects influences the hyperfine parameters, namely hyperfine induction and isomer shift. The quadrupole splitting in the ideal $L2_1$ structure should be, owing to cubic symmetry, zero. The spectra of the DAM and DIM samples measured using γ-rays in the backscattering geometry with a depth sensitivity of about 30 μm are shown in Figs. 4a and 4b and compared with the spectrum of the R sample, at the bottom in the same figure, obtained in transmission geometry. All spectra consist of the magnetically split component which was fitted using four six-line sub-components yielding the best result. The values of the hyperfine induction, isomer shift and relative area for individual sub-spectra are summarized in Table II. They relate to different local orderings of atoms in the neighborhood of the resonating Fe atoms. The mean values of the B and δ parameters and a ratio of intensities of the second and the first Mössbauer line, D_{21}, are presented in Table III. The D_{21} reflects the orientation of magnetic moments in the sample with respect to the direction of the γ-rays and as it follows from the table it is markedly influenced by technology.

The spectrum of the R sample shown in Fig. 4c differs from both DAM and DIM samples by a presence of about 15% of the paramagnetic component represented by two double- and one single-line component of hyperfine parameters; δ = 0.192(4) mm/s, Δ = 0.517(9) mm/s, δ = 0.660(59) mm/s, Δ = 1.831(110) mm/s, for the doublets and δ = 0.233(7) mm/s for the singlet. This paramagnetic component can be, at present only speculatively, ascribed to chemical and topological surface disorder and surface oxidation. The paramagnetic component formed by the doublet and singlet of similar parameters was also observed in Mössbauer spectrum of the Co_2FeAl nanoparticles prepared by co-precipitation and thermal deoxidation procedure,[14] where the surface phenomena were taken into account because of the high surface area of nanoparticles. Nevertheless, contrary to present spectra analysis, the authors in Ref. 14 have detected only one sextuplet of hyperfine parameters, B = 33 T, δ = 0.126 mm/s, and Δ = 0.002 mm/s, ascribed to a crystalline ferromagnetic phase.

TABLE II. The hyperfine parameters: hyperfine induction, B; isomer shift, δ; relative intensity, A; of individual analyzed component.

Comp.	1			2			3			4		
Sample	B (T)	δ (mm/s)	A (%)	B (T)	δ (mm/s)	A (%)	B (T)	δ (mm/s)	A (%)	B (T)	δ (mm/s)	A (%)
DAM	31.93 ±0.12	0.042 ±0.007	25.5 ±3.0	30.17 ±0.11	0.043 ±0.015	51.9 ±3.3	29.52 ±0.31	−0.173 ±0.046	9..2 ±2.8	29.37 ±0.34	0.220 ±0.052	13.4 ±2.5
DIM	32.78 ±.18	0.043 ±0.011	4.9 ±1.0	31.23 ±0.09	0.047 ±0.002	45.2 ±4.0	30.26 ±0.13	0.068 ±0.003	40.4 ±4.0	29.14 ±0.18	0.064 ±0.008	9.5 ±3.2
R	31.81 ±0.05	0.017 ±0.003	19.0 ±1.6	30.66 ±0.02	0.031 ±0.002	49.9 ±1.4	29.50 ±0.09	0.040 ±0.005	13.5 ±1.0	27.96 ±0.21	0.003 ±0.002	2.7 ±0.6

TABLE III. The mean values of hyperfine parameters; B_{mean}, δ_{mean}, and intensity ratio, D_{21}, of the second and the first Mössbauer line.

Sample	B_{mean} (T)	δ_{mean} (mm/s)	D_{21}
DAM	30.45 ± 0.03	0.047 ± 0.003	0.315 ± 0.009
DIM	30.71 ± 0.01	0.057 ± 0.007	0.509 ± .005
R	30.65 ± 0.01	0.028 ± 0.003	0.861 ± 0.003

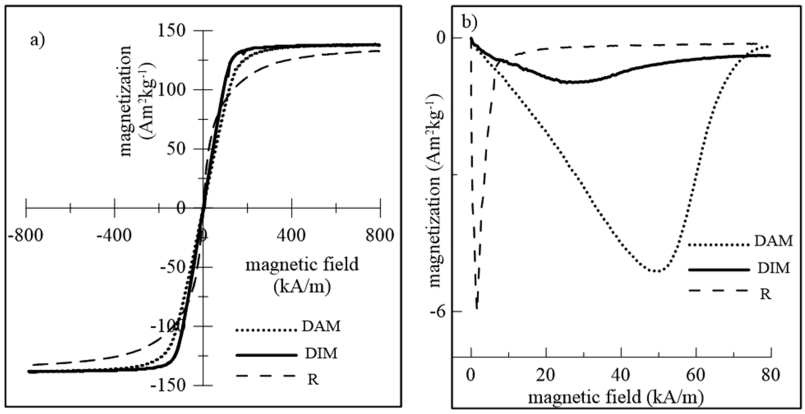

FIG. 5. Magnetic hysteresis curves (a) and Henkel plots (b) of the arc melted, DAM, induction melted, DIM, and planar flow casted, R, samples.

C. Magnetic measurements

The bulk hysteresis loops for all samples are shown in Fig. 5a. The magnetic characteristics estimated from the measured curves are summarized in Table IV. The saturation magnetization of the DAM and DIM samples are nearly the same. However, the more sensitive structural parameters, M_r and H_c, are higher for the DAM sample due to dendrites observed in grains of this sample by SEM. Lower saturation magnetization of the R sample is caused by a higher content of Al at the expense of Fe and Co, as confirmed by EDX analysis.

The $\Delta M(H)$ calculated for all samples using equation (1) is graphically represented as Henkel plots in Fig. 5b. They are negative that is an evidence of prevailing magnetic dipolar (magnetostatic dipole-dipole) interactions. They are produced by the magnetic moment of each grain and depend on the number of Fe and Co atoms present. The highest intensity $\Delta M(H)$ = -6.01 Am^2/kg, and, simultaneously, the peak position at very low magnetic field of 1.59 kA/m were obtained for R sample. This sample is characterized by the highest remanence (2.391 Am^2/kg) and the low coercivity (0.84 kA/m) value being between those for the DAM and the DIM sample. The $\Delta M(H)$ obtained for DAM sample is only slightly lower as compared to R sample whereas the required magnetic field is several times higher (see Table IV). The weakest dipolar interactions are observed in the DIM sample. The DAM and DIM samples differ in grain size and therefore it is important to take also into account exchange interactions between the neighboring grains which are defined as the exchange coupling of magnetic moments located at grain interface while the grains are in direct contact with each other. Despite the size of grains at the DAM and DIM samples being nearly the same, in the DIM sample the effect of exchange coupling is stronger than that of the magnetostatic interaction. In case of the DAM sample, it can be speculated that the dendrites decrease the effect of exchange coupling and therefore the dipolar interactions prevail. Similar behaviour was also observed for the arc melted and planar flow casted Co_2FeSi samples.[24]

The surface hysteresis loops of the DAM sample presented in Fig. 6 were taken from the spot of about 300 μm in diameter and penetration depth of about tens of nm. It was measured at the oblique

TABLE IV. Magnetic parameters derived from the VSM hysteresis loops: coercivity, H_c; saturation, M_s, and remnant, M_r, magnetization. Peak position, ΔH, and intensity, ΔM, of the Henkel plots.

Sample	DAM	DIM	R
M_s (Am^2/kg)	137.57	138.26	132.82
M_r (Am^2/kg)	1.291	0.860	2.391
H_c (kA/m)	1.30	0.69	0.84
ΔH (kA/m)	49.36	25.47	1.59
ΔM (Am^2/kg)	-5.13	-0.98	-6.01

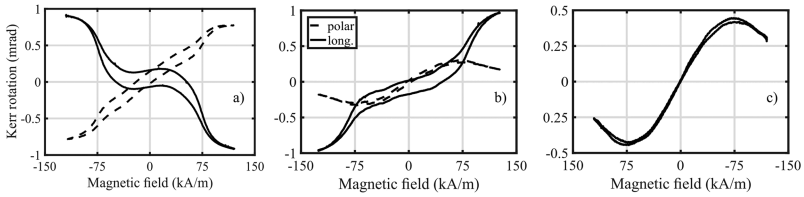

FIG. 6. Surface MOKE hysteresis loops of polished arc melted, DAM, sample; a) hysteresis loops in longitudinal configuration mutually distinguished by rotation of the sample and magnetic field by 180°, b) separated longitudinal and polar magnetization components, c) measured polar magnetization component at normal incidence geometry.

incident angle of 50° and with the magnetic field applied parallel to the plane of light incidence - longitudinal configuration (Fig. 6a). After the loop depicted by a full line was measured, the sample and magnetic field were rotated by 180° and the next loop (dashed line) was taken from the same place. Due to the symmetry of permittivity tensor of cubic crystal the contributions of the in-plane M_L (longitudinal) and out-of-plane M_P (polar) magnetization component can be easily distinguished by subtracting and adding both loops from Fig. 6a and dividing by 2. This is shown in Fig. 6b confirming the presence of both mentioned magnetization components. The out-of-plane M_P component yields faster reversal and the saturation in the 75 kA/m magnetic field. On the other hand, the in-plane M_L component is not completely saturated even in the maximal applied 125 kA/m magnetic field. The shapes and saturation effects of magnetization components may differ in the local sample places owing to imaging different grains with various anisotropies under the laser spot. The second in-plane magnetization component called transversal was separated in a similar way (not presented), but its contribution was significantly lower as compared to the longitudinal one. The in-plane magnetization component falls down to zero at the normal incidence geometry (Fig. 6c) and the polar component reaches its maximal effect of 0.44 mrad at about 75 kA/m magnetic field. Similar MOKE loops were measured also for the DIM sample in the present study and previously presented for the Co_2FeSi Heusler alloy in Ref. 24.

The hysteresis loop of the R sample measured in longitudinal configuration with magnetic field applied along the ribbon axis is presented in Fig. 7. Co_2FeAl ribbon is magnetically softer being saturated at a markedly lower magnetic field than DAM and DIM samples. Due to the preparation technology and low ribbon thickness (about 20 μm) the magnetization lies in the ribbon plane and no M_P component was detected. The shape and magnetic parameters of the loop are again strongly dependent on the local surface place illuminated by the laser spot.

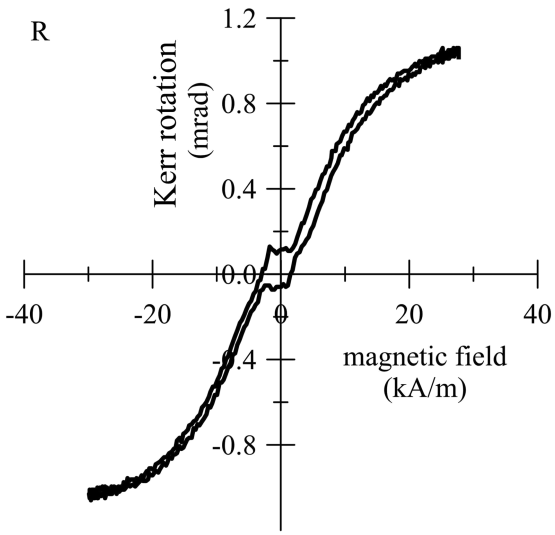

FIG. 7. Longitudinal magneto-optical hysteresis loop of ribbon, R, sample.

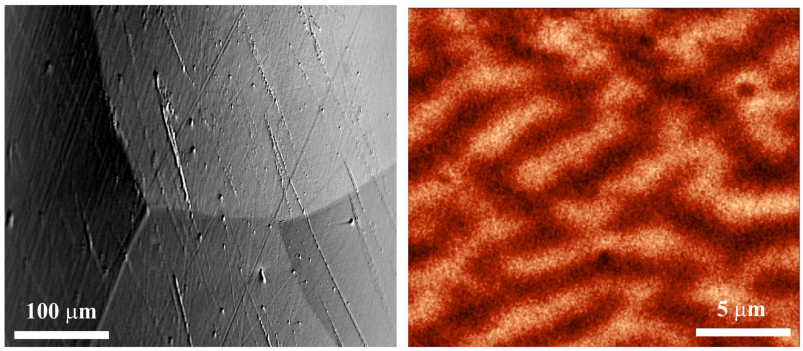

FIG. 8. Surface domain structure of DAM sample obtained by MOKM (left) and a detail taken by MFM inside the grain (right).

The surface magnetic domain structures of both DAM and DIM samples in the remnant state were very similar and therefore the images taken by the MOKM and MFM at the DAM are only shown in Fig. 8. The sample surface had to be carefully grinded and polished so that the domain structure observations could be done. The surface treatment could not be done at the very brittle R sample and the high surface roughness of both sides did not allow any domain observations. The MOKM in longitudinal configuration has yielded single-domain structure inside the grains. On the other hand, the MFM with a higher resolution has shown that the domains inside grains are formed by several fine stripe-type domains. Because the MFM technique is highly sensitive to an out-of-plane magnetization component[25] it can be expected that the observed fine domain structure originates mainly from the M_P component detected by the magneto-optical magnetometry.

IV. CONCLUSIONS

Present studies were devoted to the structural and magnetic properties of the Co_2FeAl Heusler alloys prepared by three technologies: arc melting, induction melting, and planar flow casting. The results obtained by both bulk and surface sensitive methods have documented an influence of the technological procedure on the structure and magnetic properties. The conventional technologies provided the coarse-grained samples (DAM and DIM) with only a slight difference in magnetic properties. The planar flow casting technology, not commonly applied for production of Heusler alloys, has appeared to be applicable. It resulted in the fine-grained ribbon-type sample (R) with the magnetic properties only slightly different compared to the DAM and/or DIM sample owing to the substantially smaller grains and different shape anisotropy influenced by its form. The main disadvantage was its brittleness making the manipulation with the sample difficult and its surface roughness inhibiting domain structure observations.

ACKNOWLEDGMENTS

This work was supported by the Regional Materials Science and Technology Centre - Sustainability Program (No. LO1203) and the CEITEC 2020 - National Sustainability Programme II (No. LQ1601), both funded by Ministry of Education, Youth and Sports of the Czech Republic, by the project SP2017/42, and by the Slovak research and development agency - projects Nos. VEGA 2/0082/17 and APVV-15-0049. The authors thank M. Hapla (IPM) for magnetic measurements.

[1] T. Graf, J. Winterlik, L. Müchler, G. H. Fecher, C. Felser, and S. S. P. Parkin, in *Handbook of Magnetic Materials*, 21, ed. K. H. J. Buschow, Elsevier (2013) pp. 1–76.
[2] T. M. Nakatani, Z. Gercsi, A. Rajanikanth, Y. K. Takahashi, and K. Hono, J. Phys. D: Appl. Phys. **41**, 225002 (2008).
[3] T. Ishikawa, H.-X. Liu, T. Taira, K.-I. Matsuda, T. Uemura, and M. Yamamoto, Appl. Phys. Lett. **95**, 232512 (2009).
[4] M. Julliere, Phys. Lett. A **54**, 225 (1975).
[5] W. Wang, H. Sukegawa, R. Shan, S. Mitani, and K. Inomata, Appl. Phys. Lett. **95**, 182502 (2009).
[6] W. Wang, E. Liu, M. Kodzuka, H. Sukegawa, M. Wojcik, E. Jedryka, G. H. Wu, K. Inomata, S. Mitani, and K. Hono, Phys. Rev. B **81**, 140402 (2010).
[7] S. Mizukami, D. Watanabe, M. Oogane, Y. Ando, Y. Miura, M. Shirai, and T. Miyazaki, J. Appl. Phys. **105**, 07D306 (2009).

[8] N. I. Kourov, V. V. Marchenkov, A. V. Korolev, L. A. Stashkova, S. M. Emel'yanova, and H. W. Weber, Phys. Sol. State **57**, 70 (2015).
[9] M. Hakimi, P. Kameli, H. Salamati, and Y. Mazaheri, Powder Metallurgy **56**, 11 (2013).
[10] Z. G. Zheng, X. C. Zhong, Y. H. Zhang, H. Y. Yu, and D. C. Zeng, J. Alloys Compd. **466**, 377 (2008).
[11] S. Qiao, S. Nie, Y. Yhao, and X. Zhang, J. Appl. Phys. **13**, 233914 (2013).
[12] A. Kumar and P. C. Srivastava, Material Sci.-Poland **31**, 501 (2013).
[13] K. R. Sapkota, P. Gyawali, A. Forbes, I. L. Pegg, and J. Philip, J. Appl. Phys. **111**, 123906 (2012).
[14] J. H. Du, Y. L. Zuo, Z. Wang, J. H. Ma, and L. Xi, J. Mater. Sci. Technol. **29**, 245 (2013).
[15] HighScorePlus PANalytical B.V., Almelo, The Netherlands and R. A. Young (ed.), in: The Rietveld Method, International Union of Crystallography, Book Series, Oxford University Press, 1993.
[16] ICSD Database, Version 1.9.4., 2014-1, NIST/FIZ (www.fiz-karlsruhe.de/icsd.html).
[17] T. Zak and Y. Jiraskova, Surf. Interf. Anal. **38**, 710 (2006).
[18] O. Henkel, Phys. Stat. Sol. **7**, 919 (1964).
[19] S. Thamm and J. Hesse, J. Magn. Magn. Mater. **154**, 254 (1996).
[20] Y. Takamura, R. Nakane, and S. Sugahara, J. Appl. Phys. **107**, 09B111 (2010).
[21] K. H. J. Buschow, P. G. van Engen, and R. Jongebreur, J. Magn. Magn. Mat. **38**, 1 (1983).
[22] P. J. Webster, J. Phys. Chem. Solids **32**, 1221 (1971); K. R. A. Ziebeck and P. J. Webster, J. Phys. Solids **35**, 1 (1974).
[23] Y. Takamura, R. Nakane, and S. Sugahara, J. Appl. Phys. **105**, 07B109 (2009).
[24] A. Titov, O. Životský, A. Hendrych, D. Janičkovič, J. Buršík, and Y. Jirásková, Acta Phys. Pol. A **131**, 654 (2017).
[25] D. Wu, T. Jin, Y. Lou, and F. Wei, Appl. Surf. Sci. **346**, 567 (2015).